TDI Brooks
Scientific Services on a Global Basis
TDI-Brooks International, Inc.
14391 S. Dowling, College Station, TX 77845
Ph: (979) 693-3446 Fax: (979) 693-6389
www.tdi-bi.com

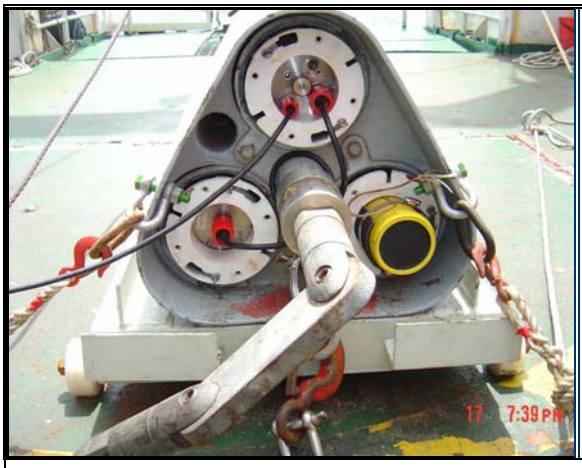

Classification Method for Identifying Potential Bottom Water Temperature Transient Sites

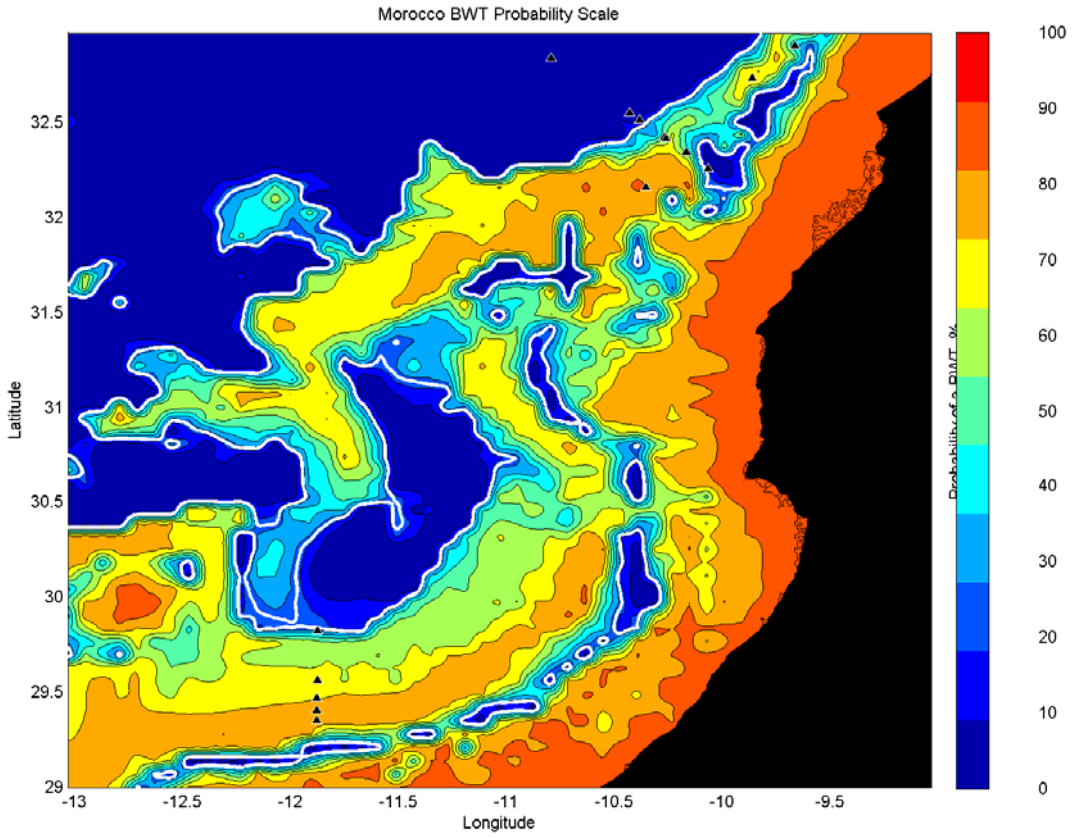

Technical Note

L.C. Bender, Ph.D.

September 2015

Table of Contents

\

1 SUMMARY

TDI-Brooks now has the capability to classify whether a potential heat flow site may be subject to a transient in the bottom water temperature. The method will correctly classify a heat flow site as stable or unstable with an accuracy exceeding 90%. The purpose of this technical note is to present the method.

For more information please contact Dr. Les Bender at +1 979.693.3446 or lesbender@tdi-bi.com.

2 INTRODUCTION

Obtaining a reliable geothermal heat flow estimate in ocean sediments is dependent on a combination of overlapping technological, geological, and oceanographic factors. The long-term temperature stability of the overlying water column is one such critical factor. Until now, it was not possible to pre-determine, as part of site selection, whether the site would have a stable bottom water temperature regime. The most reliable method was to simply avoid doing heat flow in water depths less than 600 - 800 meters. But in many cases even a deep site isn't a guarantee of a stable thermal environment.

Bottom water temperature transients have typically been identified after the fact, by recognizing a deviation from linearity in the Bullard plot and then explaining the deviation as a probable transient in the temperature of the overlying water. But it is possible to examine the bottom water temperature output of a real-time ocean model and reliably identify potential sites where transients could be expected to be a problem.

2.1 BACKGROUND

The bottom water temperature (BWT) controls the boundary condition for conduction of geothermal heat upward through the sediments. Understanding how changes to the BWT can affect a computed heat flow value is extremely important. If the BWT cools or heats suddenly, then this sends a temperature anomaly propagating by conduction downward into the sediments. Sometimes such changes in the BWT are responsible for large variations over the length of the 5-m probe, particularly at shallow water sites. TDI-Brooks recommends that heat flow be conducted in depths greater than 800 m because of the high risk of a BWT variation in shallow water. Normally in the deep ocean the BWT is fairly stable with depth, and varies only slightly in time. This is conducive to highly accurate and precise heat flow measurements. But BWTs may not be stable at any depth depending on the oceanographic factors.

Carslaw and Jaeger, 1959 present solutions of the conduction of heat into a semi-infinite solid that incorporates a background vertical temperature gradient, i.e. the geothermal background heat flux, and a temporal surface temperature forcing that is a harmonic function of time.

$$T(z,t) = T_{surface} + Gz + A_a e^{-z/\lambda_a} * \cos(\omega_a t - \frac{z}{\lambda_a} - \phi_a) + A_s e^{-z/\lambda_S} * \cos(\omega_s t - \frac{z}{\lambda_s} - \phi_s) \quad (1)$$

where $\lambda = \sqrt{2\kappa/\omega}$ is the harmonic penetration length, κ is the thermal diffusivity, *G* is the background vertical temperature gradient and *z* is positive down. The amplitude of the harmonic signal decays exponentially with depth.

An estimate of the period of the signal needed to penetrate into the sediment to a depth where the signal amplitude is 5% of the surface value can be readily made from equation (1). **Table 1** shows the results where the thermal diffusivity is based on a thermal conductivity of 1.0 W m^{-1} K^{-1}. The standard model of Villinger & Davis (1987a) relates the conductivity to the diffusivity.

Table 1. Harmonic Penetration Depth.

Signal	Period, days	Penetration Depth, meters
Semidiurnal	0.5	0.20
Fortnightly	14	1.00
Semiannual	180	3.75
Annual	365	5.35
Decadal	10 years	17.00

These transients, depending on the amplitude and frequency, can, and do, affect the heat flow calculations. *Longer period signals have the greatest potential to affect the heat flow since they can cause significant temperature variations over the length of a 5-m heat flow probe.* Long period signals are an immediate concern because they have the potential to distort the computed heat flow value.

2.2 METHOD

The method utilizes the bottom water temperature output of a real-time ocean model in order to identify potential sites where bottom water temperature transients could be expected to distort heat flow values. The purpose of this section is to describe the six steps that comprise the method.

Step 1) Retrieve the bottom water temperature history from archived runs of a numerical ocean model.
Step 2) Use an FFT to extract the peak frequencies.
Step 3) Use the peak frequencies to fit a sinusoidal model to the temperature history.
Step 4) Use the amplitude and phase information from the sinusoidal model to compute a simulated vertical temperature profile time series.
Step 5) Compute the heat flow based on the deepest five thermistors.
Step 6) Rank the probability the site will be affected based on the percentage of time the computed heat flow is greater or less than of the assumed initial background value of 40 m W m^{-2}.

2.2.1 Step 1

The bottom water temperatures are retrieved from archived runs of the HYCOM 2.2 eddy-resolving, ocean numerical model. The model is run every six hours at the US Navy Supercomputing Resource Center. Computations are carried out on a Mercator grid between 78°S and 47°N (1/12° equatorial resolution). The horizontal dimensions of the global grid are 4500 x 3298 grid points resulting in ~7 km spacing on average. There are 32 vertical layers. Surface forcing is from NAVy Global Environmental Model (NAVGEM) version 1.2 and includes wind stress, wind speed, heat flux (using bulk formula), and precipitation. Experience with this model has shown it is surprisingly reliable as a proxy model for calculating sound velocity profiles. **Figure 1** shows the retrieved temperature history (blue line) for a representative site off the southwestern coast of Portugal. The model depth is 1000m. Presumably this is deep enough to be immune to a BWT transient, but the influence of the Mediterannean Outflow, an oceanographic factor, cannot be discounted.

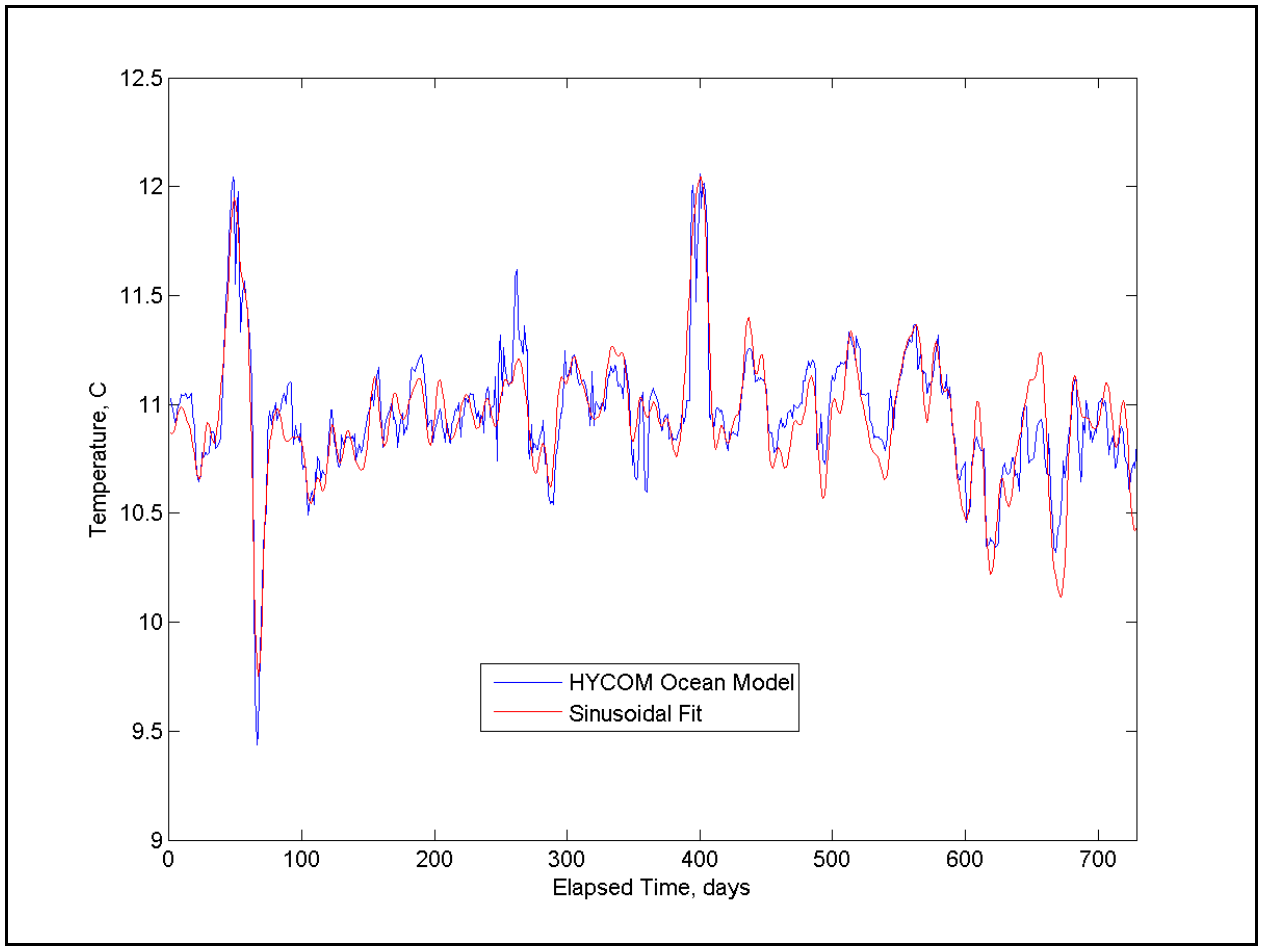

Figure 1: Bottom water temperature history

2.2.2 Step 2

The spectrum of the bottom water temperature history is computed using a covariance approach, rather than a Fast Fourier Transform (FFT). Because of the short sample length, 729 data points, and fast computational speeds of today's computers there is no need to use an FFT to extract the spectrum. A major advantage of the covariance approach is the frequency range can be pre-determined. **Figure 2** shows the corresponding spectra for the example for the representative site shown in **Figure 1**. The first six peak frequencies are shown in **Table 2**, along with the amplitude determined in *Step 3*. The magnitude of the amplitude is important because it is the combination of frequency and amplitude that punches the temperature excursion down into the sediment.

Table 2. Frequency, period and amplitude

Frequency, cpd	Period, days	Amplitude, C
0.0283	35.4	0.143
0.0232	43.1	0.141
0.0017	597	0.133
0.0199	50.3	0.108
0.0058	173	0.102
0.0116	86.4	0.090

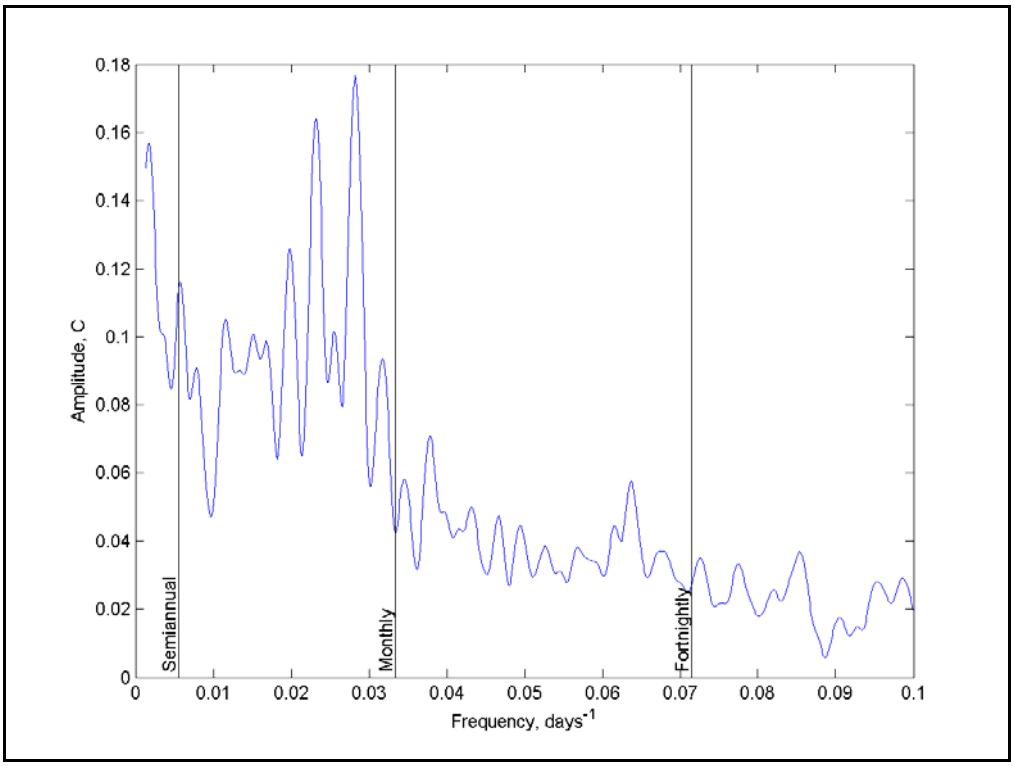

Figure 2: Spectra of bottom water temperature history showing the fortnightly, monthly and semiannual periods.

2.2.3 Step 3

The peak frequencies determined in *Step 2* are used to fit a sinusoidal model to the bottom water temperature history. **Figure 1** shows the sinusoidal fitted temperature history (red line) for the representative site off the southwestern coast of Portugal. The average bias between the sinusoidal fit and the HYCOM model temperature history is 0.01 C. **Table 2** shows the fitted amplitudes.

2.2.4 Step 4

The amplitude and phase information from the sinusoidal model are then used to compute a simulated vertical temperature profile time series, per equation (1). **Figure 3** shows the resulting vertical temperature profile based on an assumed background heat flow of 40 $mW\ m^{-2}$.

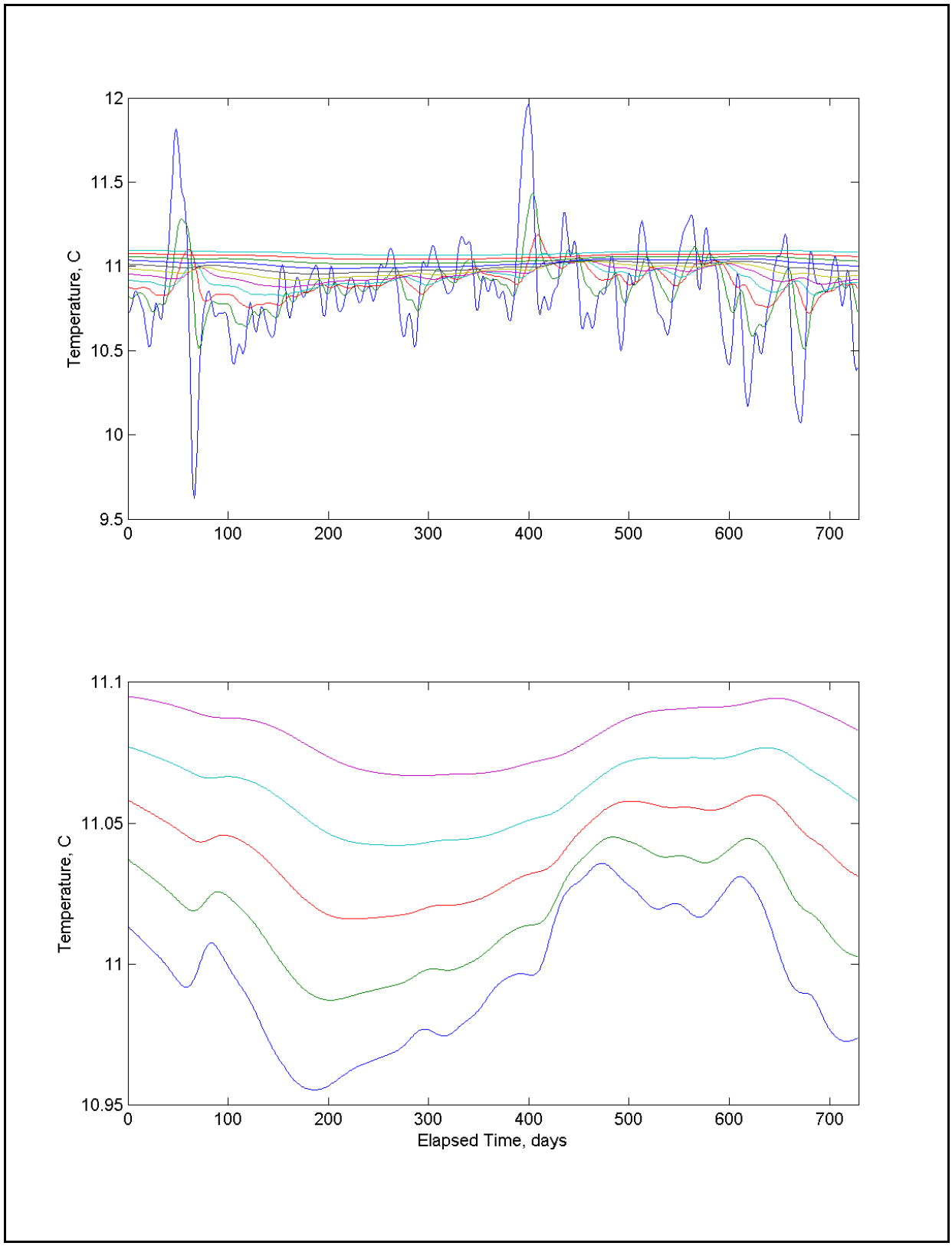

Figure 3: Simulated vertical temperature profile based on an assumed background heat flow of 40 *mW m^{-2}* and the surface forcing temperature. The top panel shows all eleven thermistors and the bottom panel shows the deepest five thermistors.

2.2.5 Step 5

The heat flow based on the simulated vertical temperature profile from the deepest five thermistors (bottom panel of **Figure 3**) is calculated. **Figure 4** shows how the heat flow will vary in time due to the bottom water temperature excursion. Depending on when the heat flow is taken it could be as high as 58.2 *mW m*$^{-2}$ (**Figure 5**) or as low as 22.2 *mW m*$^{-2}$ (**Figure 6**). One should not be persuaded to report a *reliable* heat flow based on the deepest five thermistors on the assumption they are deep enough to be unaffected by bottom water temperature variations.

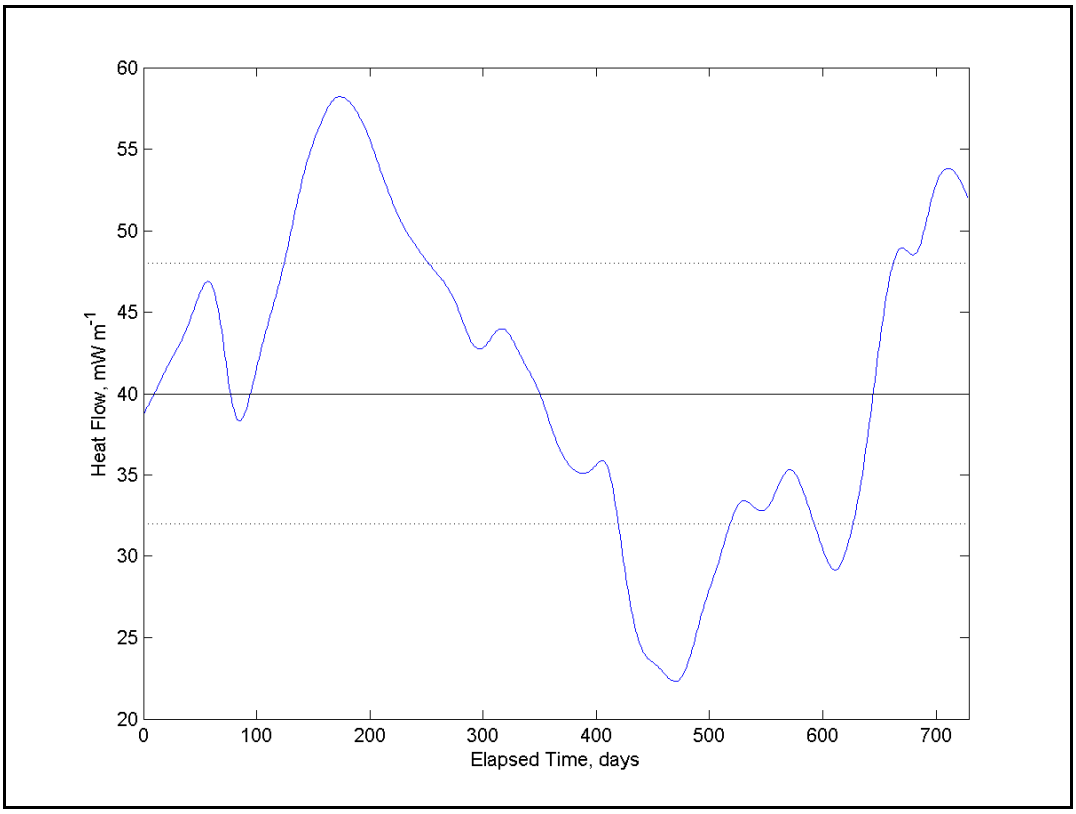

Figure 4: Simulated heat flow history.

2.2.6 Step 6

The final step ranks the probability the site will be unstable based on the percentage of time the computed heat flow is within 20% of the assumed initial background value of 40 mW m^{-2}. In this case, the ranges of a stable heat flow lies between 32 and 48 mW m^{-2}. For this example the heat flow is outside of this range 45% of the time. Anything greater than 25% is likely to result in a heat flow estimate that is significantly affected by a BWT transient. This is clearly illustrated in **Figures 5 and 6**. These are taken from the points corresponding to the maximum and minimum heat flow shown in **Figure 4**. While it is possible to draw a linear line through the deepest five thermistors and calculate a heat flow, it is not a “true” heat flow; it has been distorted by the transients in the bottom water temperature. It is even possible to get a negative heat flow.

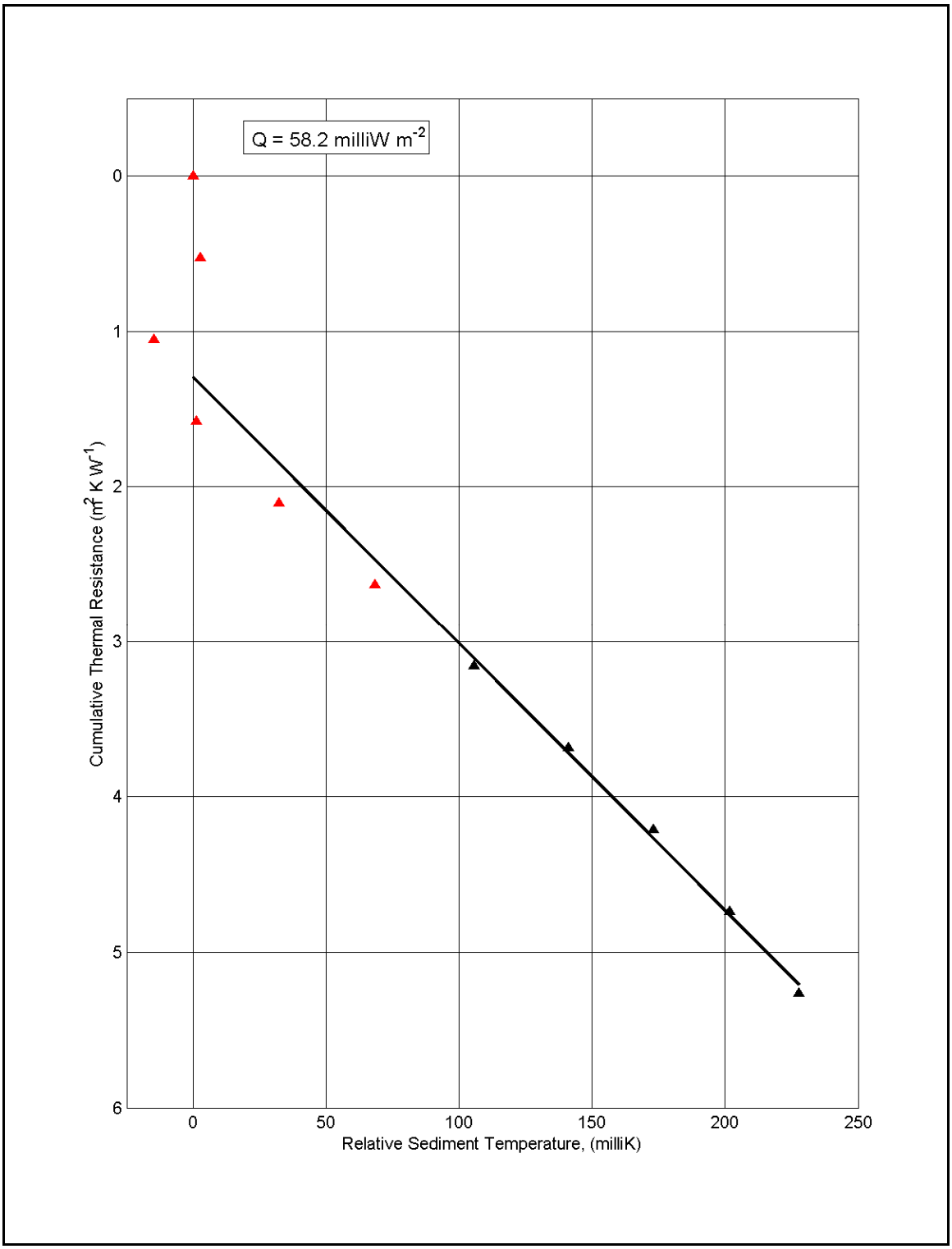

Figure 5: Estimated heat flow at the maximum.

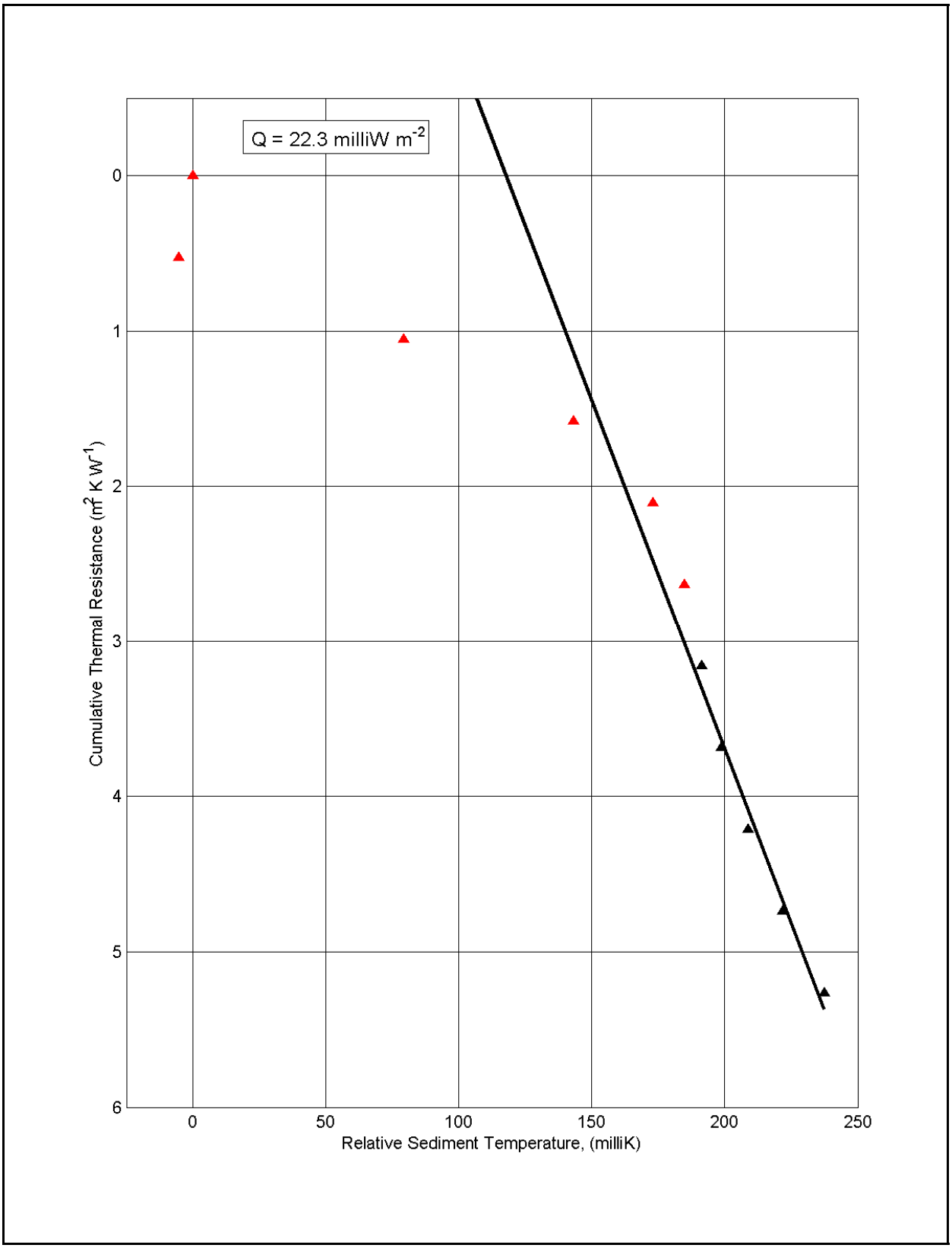

Figure 6: Estimated heat flow at the minimum

2.3 VALIDATION

Eighty-two (82) heat flow sites in four basins, Jamaica, Morocco, Tanzania, and Portugal, were randomly chosen from the large number of heat flow projects conducted by TDI-Brooks over the past 15 years. Morocco and Portugal are examples of deep sites that don't guarantee a stable thermal environment.

Each of the Bullard plots was examined for a significant departure from linearity. If this was the case, the site was labeled as a non-equilibrium heat flow site. If the Bullard plot was linear, then the site was an equilibrium heat flow. By equilibrium we mean the BWT history is stable enough so that the heat flow is in equilibrium.

The method outlined in this note was then applied to the sites. If the resulting probability for a bottom water transient was less than 30%, then this site was categorized as a stable site for a heat flow measurement. If the probability was higher than 30%, the site was categorized as unstable.

Table 3 summarizes the results. There were a total of seven (7) sites that were incorrectly identified. Either the Bullard plot was linear and the method classified the site as unstable (5 sites) or the Bullard plot was non-linear and the method classified the site as stable (two sites.)

Table 3. Site Locations.

Basin	# of HF Sites	# of Misidentified Sites
Jamaica	11	0
Morocco	13	2
Tanzania	46	4
Portugal	12	1
Total	82	7

Figures 7 - 10 and **Tables 4- 7** provide the specific details for each of the four basins.

2.3.1 Jamaica

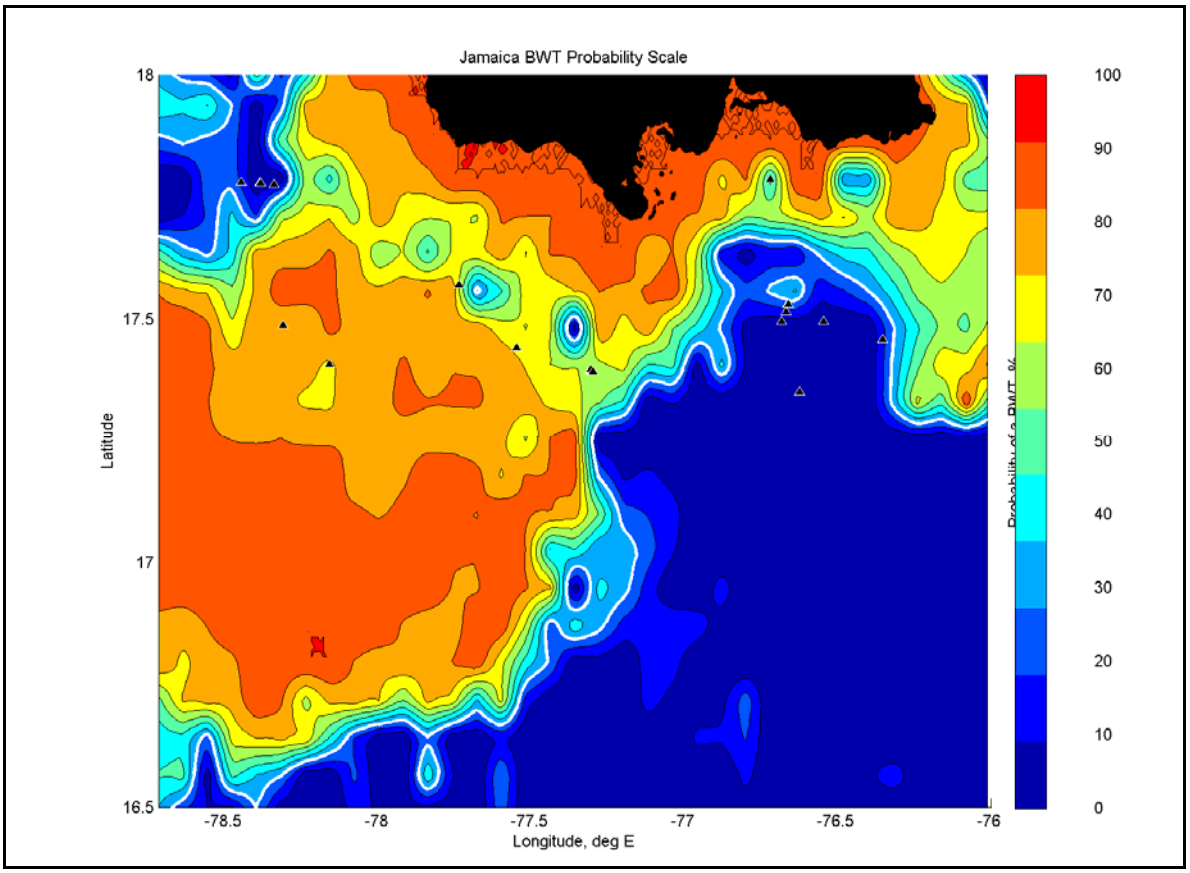

Figure 7: Probability of a BWT transient offshore of Jamaica. The heat flow sites are denoted with a black triangle. The solid white line is the 30% contour line.

Table 4. Jamaica Heat Flow

Station ID	Bullard Plot	Depth, m	BWT Probabiity, %
HF 1a	Equilibrium heat flow	2003	18.08
HF 2a	Equilibrium heat flow	2002	2.88
HF 2b	Equilibrium heat flow	2089	0.00
HF 3	Equilibrium heat flow	1600	18.68
HF 4 Alt	Non-equilibrium heat flow	1358	44.62
HF 6	Non-equilibrium heat flow	1301	78.09
HF 9	Non-equilibrium heat flow	924	71.36
HF 10	Non-equilibrium heat flow	1635	35.72
HF 11	Equilibrium heat flow	1437	18.94
HF 12	Equilibrium heat flow	1614	3.09
HF 13	Equilibrium heat flow	2012	7.64

2.3.2 Morocco

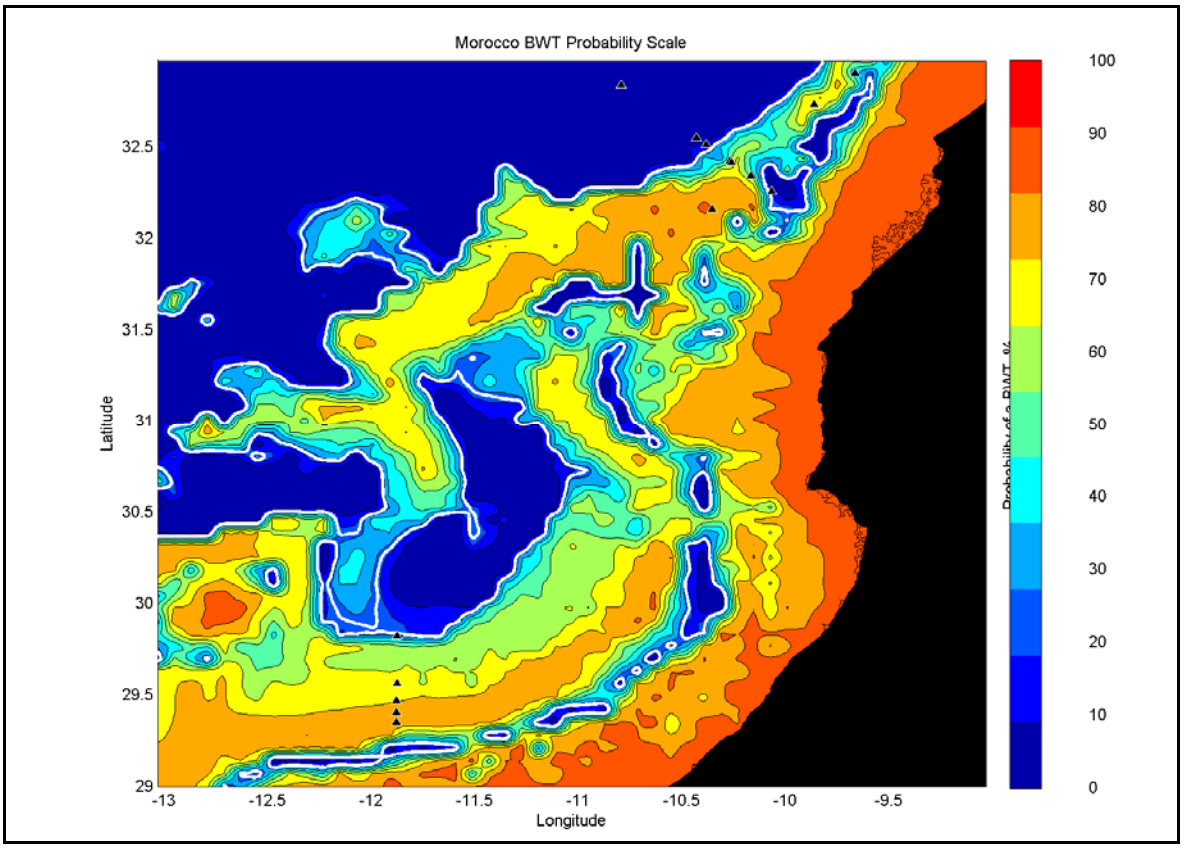

Figure 8: Probability of a BWT transient offshore of Morocco. The heat flow sites are denoted with a black triangle. The solid white line is the 30% contour line.

Table 5. Morocco Heat Flow

Station ID	Bullard Plot	Depth, m	BWT Probabiity, %
CWD01HF	Equilibrium heat flow.	4316	0.00
CCD02HF	Non-equilibrium heat flow	2134	42.99
CCD04HF	Non-equilibrium heat flow	2295	88.95
CCD05HF	Equilibrium heat flow.	2508	77.21
CWD08HF	Equilibrium heat flow.	3510	3.23
CWD09HF	Equilibrium heat flow.	3654	9.21
CCD11HF	Non-equilibrium heat flow	2806	61.50
CCD12HF	Equilibrium heat flow.	2094	14.16
CRD13HF	Equilibrium heat flow.	1465	86.11
CRD14HF	Non-equilibrium heat flow	1575	85.00
CRD15HF	Non-equilibrium heat flow	1617	79.39
CRD16HF	Non-equilibrium heat flow	1812	72.67
CRD17HF	Non-equilibrium heat flow	2038	32.31

2.3.3 Tanzania

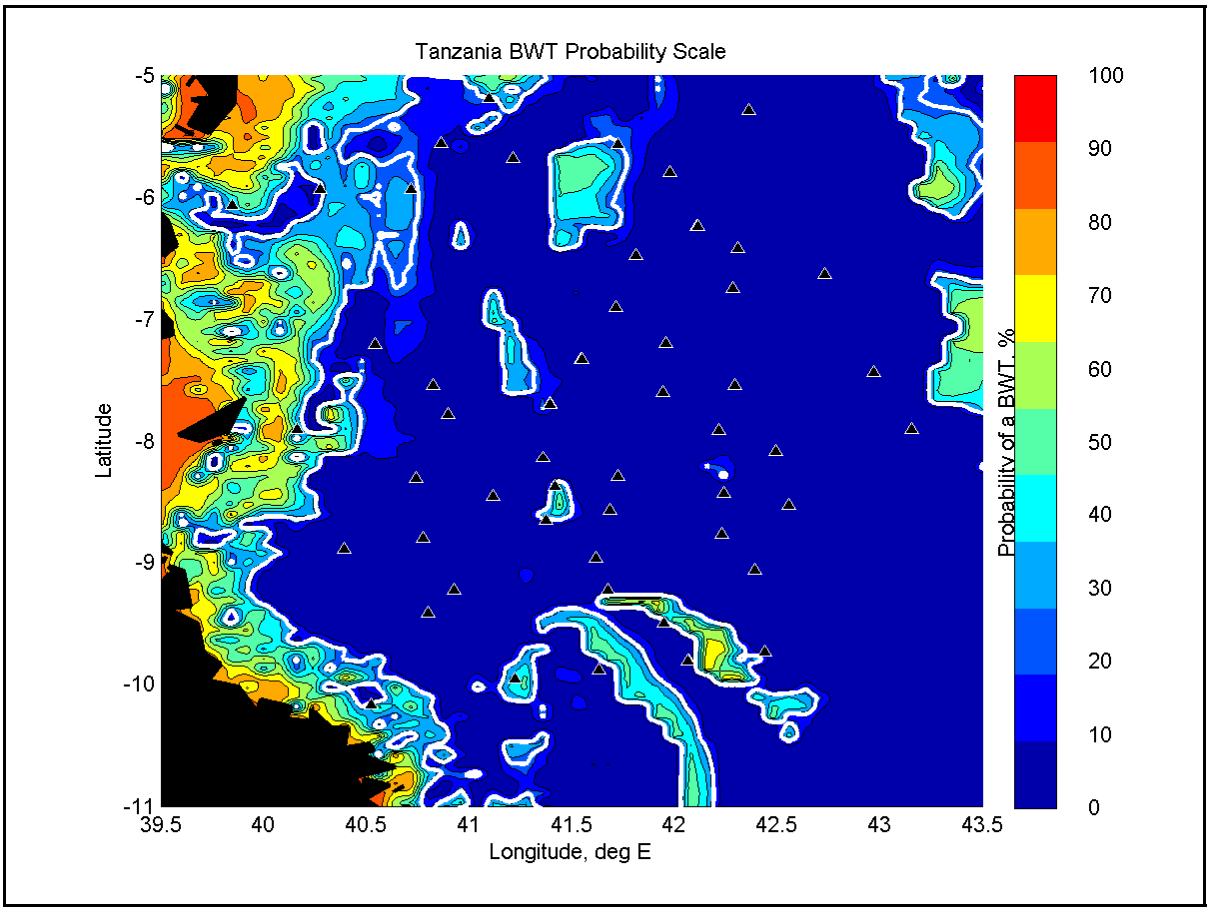

Figure 9: Probability of a BWT transient offshore of Tanzania. The heat flow sites are denoted with a black triangle. The solid white line is the 30% contour line

Table 6. Tanzania Heat Flow

Station ID	Bullard Plot	Depth, m	BWT Probability, %
TZH002	Equilibrium heat flow	2265	0.13
TZH003	Equilibrium heat flow	3128	6.85
TZH004	Equilibrium heat flow	2932	15.06
TZH006	Equilibrium heat flow	3036	0.00D
TZH007	Equilibrium heat flow	3460	0.00
TZH009	Equilibrium heat flow	3009	0.00
TZH010	Equilibrium heat flow	3433	0.00
TZH011	Equilibrium heat flow	3552	0.00
TZH012	Equilibrium heat flow	2796	0.00
TZH013	Equilibrium heat flow	2916	19.61
TZH014	Equilibrium heat flow	3133	0.00
TZH015	Equilibrium heat flow	3421	0.00
TZH016	Equilibrium heat flow	2822	0.00

Station ID	Bullard Plot	Depth, m	BWT Probability, %
TZH017	Equilibrium heat flow	3049	0.00
TZH018	Equilibrium heat flow	3186	0.00
TZH019	Equilibrium heat flow	3657	0.00
TZH021	Equilibrium heat flow	2556	0.00
TZH022	Equilibrium heat flow	2947	0.00
TZH023	Equilibrium heat flow	3503	0.00
TZH024	Equilibrium heat flow	2633	0.00
TZH025	Equilibrium heat flow	2966	14.81
TZH026	Equilibrium heat flow	3321	0.00
TZH027	Equilibrium heat flow	3491	0.00
TZH028	Equilibrium heat flow	3840	0.00
TZH029	Equilibrium heat flow	2383	1.57
TZH030	Equilibrium heat flow	2942	0.00
TZH031	Equilibrium heat flow	3337	0.00
TZH032	Equilibrium heat flow	3061	0.00
TZH033	Equilibrium heat flow	3461	0.00
TZH034	Equilibrium heat flow	3754	0.00
TZH035	Equilibrium heat flow	3214	0.76
TZH036	Equilibrium heat flow	3540	0.00
TZH037	Equilibrium heat flow	3323	0.00
TZH038	Equilibrium heat flow	2772	0.15
TZH039	Non-equilibrium heat flow	3542	1.25
TZH040	Equilibrium heat flow	3156	24.96
TZH041	Equilibrium heat flow	3350	0.00
TZH042	Equilibrium heat flow	1756	2.66
TZH043	Equilibrium heat flow	1273	50.46
TZH044	Equilibrium heat flow	2540	0.00
TZH046	Equilibrium heat flow	2742	0.00
TZH047	Equilibrium heat flow	2300	21.74
TZH048	Equilibrium heat flow	2295	7.43
TZH049	Possible non-equilibrium	1943	29.95
TZH050	Non-equilibrium heat flow	1770	22.12
TZH051	Equilibrium heat flow	1465	42.24

2.3.4 Portugal

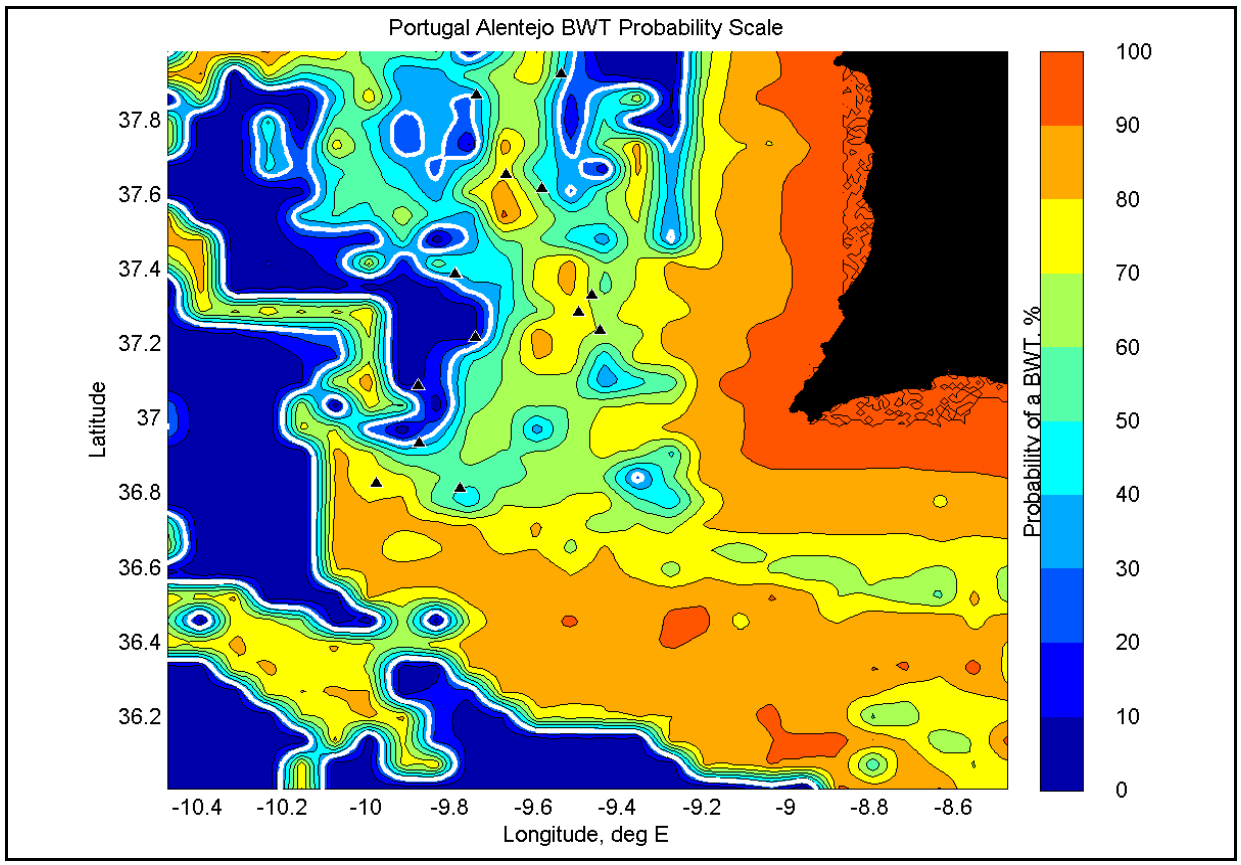

Figure 10: Probability of a BWT transient offshore of Portugal. The heat flow sites are denoted with a black triangle. The solid white line is the 30% contour line

Table 7. Portugal Alentejo Heat Flow

Station ID	Bullard Plot	Depth, m	BWT Probabiity, %
HF-PPF-c	Non-equilibrium heat flow	1452	78.31
HF-PPF-e	Non-equilibrium heat flow	1121	67.81
HF-PPF-f	Non-equilibrium heat flow	2170	38.33
HF-PPF-g	Non-equilibrium heat flow	2751	72.57
HF-PPF-h	Non-equilibrium heat flow	2475	55.93
HF-PPF-i	Equilibrium heat flow	3304	17.13
HF-PPF-j	Equilibrium heat flow	3429	33.60
HF-PPF-k	Non-equilibrium heat flow	1247	78.63
HF-PPF-l	Non-equilibrium heat flow	1197	63.47
HF-PPF-n	Non-equilibrium heat flow	1423	50.13
HF-PPF-o	Non-equilibrium heat flow	1332	47.07
HF-PPF-p	Non-equilibrium heat flow	2140	41.51

REFERENCES

Carslaw, H.S. and J.C. Jaeger, Conduction of Heat in Solids, 2nd Edition, Oxford at the Clarendon Press, 1959.

Villinger, H. and E.E. Davis, A new reduction algorithm for marine heat flow measurements, Journal of Geophysical Research, **92**, 12,846-12,856, 1987a.